Title: A single amino acid in RTEL1 determines telomere length in mice

Authors: Riham Smoom[1†], Catherine Lee May[2†], Hannah Kolev[2], Yitzhak Reizel[2], Ashleigh Morgan[2], Klaus H. Kaestner[2*] and Yehuda Tzfati[1*]

Affiliations:

[1]Department of Genetics, The Silberman Institute of Life Sciences, The Hebrew University of Jerusalem; Safra Campus, Jerusalem, 91904, Israel.

[2]Department of Genetics and Institute for Diabetes, Obesity and Metabolism, Perelman School of Medicine, University of Pennsylvania; Philadelphia, PA 19104, USA.

*Corresponding authors. Email: tzfati@mail.huji.ac.il (Y.T.) and kaestner@pennmedicine.upenn.edu (K.H.K)

[†]These two authors contributed equally to this work.

ABSTRACT

Maintaining optimal telomere length throughout life limits cancer and enables healthy aging. Yet, it is unclear how the telomere length set point is determined. Telomeres in the house mouse, *Mus musculus,* are 2-4 times longer than human telomeres, limiting the use of the mouse as a model for telomere research. By introducing a single amino acid variation found in *M. spretus* into the helicase RTEL1 of *M. musculus,* we shortened its telomere length set point 2-3 times, implicating this variation in the dramatic difference in telomere length between the two mouse species. While the engineered mice are fertile and healthy, hepatocytes with short telomeres displayed reduced proliferation capacity. This 'telomouse' is a unique model for studying the implications of short telomeres in aging and cancer.

INTRODUCTION

Optimal and age-appropriate telomere length is critical for maintaining genome stability and regulating cell proliferation - the major determinants of carcinogenesis and aging [1,2]. The enzyme telomerase can elongate telomeres to compensate for sequence loss due to incomplete replication and degradation [3]. However, despite decades of research, it is not yet understood how telomere length homeostasis is achieved. The large difference (2-4-fold) in telomere length between two closely related and inter-breedable species of mice, *M. musculus* and *M. spretus,* was exploited in past attempts to identify dominant genes that determine species-specific telomere length [4,5]. Interestingly, none of the known telomere maintenance genes were identified in these screens. Instead, the difference in telomere length between the two species was associated with a single locus, encoding a DNA helicase, therefore termed 'Regulator of Telomere Length' [4,6]. However, despite much effort, the difference between the *M. musculus* and *M. spretus* RTEL1 proteins that results in the large difference in telomere length has not been identified thus far [7].

We have previously identified germline mutations in human *RTEL1* that cause the fatal telomere biology disease Hoyeraal-Hreidarsson syndrome (HHS) [8]. HHS is characterized by accelerated telomere shortening and diverse clinical symptoms including bone marrow failure, immunodeficiency, and developmental defects [9]. Other HHS-causing mutations were found in telomerase subunits or factors essential for telomerase biogenesis or recruitment to telomeres [10]. While mouse and human RTEL1 dysfunction was reported to cause genome-wide damage and telomere deletion [11-13], other reports suggested that RTEL1 is also essential for telomere elongation by telomerase [14,15]. One of the missense mutations identified in the HHS patients resulted in changing methionine 492 to an isoleucine [8]. Methionine 492 is highly conserved in the helicase domain of RTEL1 across vertebrates with a few exceptional species having a leucine at this position. *M. spretus* is the only vertebrate species having a more radical change, namely to the positively charged amino acid lysine [8]. This intriguing finding led us to hypothesize that lysine 492 in *M. spretus* might be responsible for the difference in telomere

length between the two mouse species [8]. To test this hypothesis and attempt to generate a mouse model with short telomeres, we introduced the *M. spretus* variation in RTEL1 into *M. musculus*.

RESULTS

A house mouse with short telomeres

We derived *M. musculus* mice in which amino acid 492 was changed to the lysine present in *M. spretus* using CRISPR-Cas9 assisted genome editing in zygotes (Fig. 1A). We employed Nickase (D10A Cas9 mutant) mRNA and two guide RNAs to generate nicks on both strands of the *Rtel1* gene and facilitate gene conversion using a repair template (Fig. 1B). Successful gene targeting in the resulting offspring was confirmed by DNA sequencing and by allele-specific Taqman probe-based PCR (Fig. 1C,D). This founder mouse was purified from off-target effects by backcrossing to wild-type C57BL/6 mice to generate F0 mice heterozygous for the *Rtel1*^{M492K} allele, termed *Rtel1*$^{M/K}$. F0 *Rtel1*$^{M/K}$ mice were intercrossed to generate F1 and F2 *Rtel1*$^{M/K}$. Homozygosity for the Rtel1 mutation (*Rtel1*$^{K/K}$) was established in the third generation (F3). The homozygous *Rtel1*$^{K/K}$ mice bred *inter se* for seven additional generations up to F10, and were analyzed for telomere length and function as well as growth, fertility, and physiological parameters.

In order to determine the effect of the *Rtel1*^{M492K} mutation on telomere length, we employed two experimental paradigms. First, we established fibroblast cultures from *Rtel1*$^{M/K}$ and *Rtel1*$^{K/K}$ F3 embryos generated by intercrossing F2 *Rtel1*$^{M/K}$ mice. We also obtained wild-type (WT; *Rtel1*$^{M/M}$) embryonic fibroblasts, generated from intercrossing WT mice as controls. Mouse embryonic fibroblast (MEF) cultures were established by serial passaging and selection for spontaneous immortalization, and followed in culture over 250 population doublings (PD; Fig. S1A). During growth, the cultures passed through transition points in which the MEFs increased their growth rates and changed their cell morphology (Fig. S1B,C). During the final growth phase, *Rtel1*$^{M/K}$, *Rtel1*$^{K/K}$ and *Rtel1*$^{M/M}$ (WT) MEFs grew at the same average rate (about one PD/day). We determined average telomere lengths at multiple

time points by digesting high molecular weight genomic DNA with the restriction endonuclease *HinfI*, and separating the restriction fragments by pulse-field gel electrophoresis (PFGE). The dried gel was hybridized with a telomeric C-probe, first to the native DNA to detect the telomeric single-stranded overhang and then again, after denaturation, to detect the double-stranded telomeric DNA (representative gel images are shown in Fig. 2A and Supplementary Figs. S2-4). The average mean TRF length (MTL) in the WT (*Rtel1*$^{M/M}$) MEFs was 46.9 kb at PD 10, and then it shortened during the early growth phase and stabilized at about 40 kb until PD 250 (Fig. 2A,B). In contrast, the mutant *Rtel1*$^{M/K}$ and *Rtel1*$^{K/K}$ MEFs displayed shorter telomeres at PD 10 (MTL 34.2 and 30.1 kb, respectively), and they continued to shorten gradually to 21.6 and 15.5 kb, respectively, at PD250 (Fig. 2A,B). Remarkably, most telomeric fragments (~55%) of the *Rtel1*$^{K/K}$ TRF at PD 250 were shorter than 20 kb (Fig. 2C).

Sharp clonal bands of distinct TRF lengths appeared in the *Rtel1*$^{M/K}$ and *Rtel1*$^{K/K}$ MEFs, presumably indicating gradual telomere shortening due to insufficient telomerase action at telomeres, as proposed previously for mouse embryonic stem cells null for *mRtel1* [6](Figs. 2A, S2, S3). The WT MEFs also displayed sharp bands during the initial growth phase in which mean TRF length decreased, indicating reduced telomerase action (Figs. 2A, S2E and S3). Beyond PD 70, these sharp bands largely disappeared and the telomere length stabilized, consistent with the increased telomerase activity and change of cell morphology associated with immortalization [16]. In contrast to the WT MEFs, the *Rtel1*$^{M/K}$ and *Rtel1*$^{K/K}$ mutant MEFs maintained at least some of the sharp bands up to PD 250, indicating that telomerase activity was insufficient to maintain stable telomere length. Nevertheless, the shortening of the individual *Rtel1*$^{K/K}$ bands correlated with fragment length and slowed down as they these fragments shortened (Figs. 2A, S2A,B and S3A,B), suggesting that telomerase action differentially increased in the *Rtel1*$^{K/K}$ MEFs for the shorter telomeres, as they approached mean TRF length of about 15 kb. The shorter telomeres of the *Rtel1*$^{K/K}$ MEFs are comparable in length to those of human fibroblasts immortalized by ectopic expression of telomerase [17].

Functional *Rtel1*$^{K/K}$ MEFs telomeres

The main function of telomeres is to suppress the DNA damage response (DDR) at chromosome ends, which can cause cell cycle arrest and deleterious fusions of chromosome ends and breakage of dicentric chromosomes [18]. The presence of DDR foci at telomeres, termed telomere dysfunction-induced foci (TIFs), is a hallmark of telomere failure. To examine if the telomeres of the *Rtel1*$^{K/K}$ MEFs retained their protective properties, we studied the presence of TIFs in these cells using antibodies against the DDR marker γH2AX and the telomere protein TRF2 (Fig. 2D). The overall levels of DDR were high in all MEF cultures, as reported previously for MEFs growing under atmospheric oxygen levels [19]. However, there was no significant difference in the overall number of DDR foci between the WT (*Rtel1*$^{M/M}$) and mutant (*Rtel1*$^{K/K}$) MEFs (Fig. 2E). In addition, there was no increase in TIF formation in the mutant compared to WT MEFs (Fig. 2F), indicating that the shorter *Rtel1*$^{K/K}$ telomeres were functional and suppressed DDR as well as the WT telomeres did.

Shortened telomeric overhangs are associated with telomere dysfunction in HHS patients and heterozygous carriers of the M492I mutation in *RTEL1* [8,15,20]. To test whether the *Rtel1*^{M492K} mutation in the MEFs also affected the telomeric overhang maintenance, we quantified the native in-gel hybridization signal as a measure of the average length of the G-rich single-stranded telomeric sequence. The native signal remained constant and comparable to the WT signal (Fig. S4). Thus, although the *Rtel1*^{M492K} mutation resulted in shorter telomeres, it did not compromise the telomeric overhang, which is essential for the telomere end structure.

Short telomeres in *Rtel1*$^{K/K}$ mice

Telomeres of the *Rtel1*$^{K/K}$ MEFs shortened over time in culture, as described above. However, telomere shortening in cultured fibroblasts does not necessarily imply a reduced telomere length set point in the germline and somatic tissues of the mutant mice. Therefore, we analyzed telomere length in blood and tail samples taken from *Rtel1*$^{K/K}$ mice over six (blood) or seven (tail) generations (F4 to F9 or F10,

respectively). As shown in Figure 3A,C, telomeres in the tail samples shortened with each generation, reaching an average of 23 kb in F10 mice (compared to 43 kb in the WT). The shortening rate calculated based on the best curve fit was initially about 2 kb per generation at F4, but it slowed slowed down to 0.3 kb per generation at F10 (Fig. 3C). In the blood, mean TRF length shortened about 0.7 kb per generation, reaching an average of 24 kb in F9 mice (as compared to 39 kb in the WT; Fig. 3B,D). As a reference, telomeres of *M. musculus* deleted for telomerase RNA (*mTR*$^{-/-}$) shorten by 4.8 ± 2.4 kb per generation [21]. Therefore these results indicated that telomerase activity was not completely lost but that the telomere length set point in the germline of the *Rtel1*$^{K/K}$ mice was reduced with each successive generation. Notably, nearly 40% of the telomeric fragments in the F10 (tail) and F9 (blood) were shorter than 20 kb (Fig. 3E,F). Consistent with the observation in MEFs, no reduction was observed in the native hybridization signal corresponding to the single-stranded G-rich telomeric sequences (Fig. S5), indicating that the *Rtel1*$^{K/K}$ mice maintained an intact telomere end structure.

Decreased proliferation capacity *in vivo*

The *mTR*$^{-/-}$ can be intercrossed only for six generations because of loss of fertility [21]. Cells from the fourth *mTR*$^{-/-}$ generation (G_4) onward exhibit frequent chromosome ends lacking detectable telomere repeats as well as end-to-end fusions and aneuploidy, correlating with defective spermatogenesis and reduced proliferation capacity of hematopoietic cells in the bone marrow and spleen [22]. As expected from the intact telomere end structure and function described above, *Rtel1*$^{K/K}$ mice showed normal morphology and proliferation rate in telomerase-expressing intestinal stem and progenitor cells, the fastest proliferating cells in the body (Fig. 4A). EdU positive cells were found restricted to jejunal and colonic crypts in a pattern indistinguishable from WT mice. The *mTR*$^{-/-}$ mice displayed progressive decline of the cell proliferation rate in the testes starting from G_3, reveled by five-fold reduction in BrdU-positive nuclei as compared to WT, leading to progressive depletion of germ cells and eventually infertility in G_6 [21]. To examine if the short telomeres of the *Rtel1*$^{K/K}$ mice affected spermatogenesis, we

analyzed EdU incorporation in the testes of F5 and F6 *Rtel1*$^{K/K}$ mice, and found a normal proliferation rate in the spermatogonia of the seminiferous tubules, as well as normal size and histology (Fig. 4B). While we did not observe any aberrant phenotype for the *Rtel1*$^{K/K}$ mice under normal physiological condition, we suspected that when normally quiescent somatic cells are challenged in an extreme condition requiring rapid cell renewal, we might observe a phenotype that distinguishes the *Rtel1*$^{K/K}$ mice from normal mice. Such a phenotype would indicate, as a proof of concept, that the *Rtel1*$^{K/K}$ 'telomouse' can be used as a model for studying the effect of shorter telomeres on cell proliferation, cancer and aging. To this end, we performed a competitive repopulation assay with normally quiescent adult hepatocytes. This assay takes advantage of the FAH (fumaryl acetoacetate hydrolase) null (*fah*$^{-/-}$) mouse model of conditional hepatocyte killing to drive massive expansion of transplanted hepatocytes [23]. Equal numbers of *Rtel1* WT (GFP-positive) and *Rtel1*$^{K/K}$ (F10; GFP-negative) hepatocytes were transplanted into *fah*$^{-/-}$ mice and death of host hepatocytes was induced through withdrawal of the protective drug nitisinone (Fig. 4C). The 50:50 mixture of the two genetically distinct hepatocytes was confirmed by TaqMan PCR genotyping (Fig. 4D). In this model, transplanted quiescent hepatocytes reenter the cell cycle and replicate up to 12 times in order to restore functional liver mass. Four weeks after hepatocyte transplantation, livers were harvested and the proportion of FAH-expressing GFP^{+} and GFP^{-} hepatocyte repopulation nodules was quantified. Figure 4E shows a representative section of the liver, where repopulation nodules are marked in red (indicating transplanted *FAH* cells). In addition to red, WT hepatocyte nodules (but not *Rtel1*$^{K/K}$ mutants) are marked in green. Quantifying the fraction of hepatocyte nodules over multiple liver sections, we observed a nearly two-fold decrease in the number of repopulation nodules derived from *Rtel1*$^{K/K}$ hepatocytes, as compared with the WT hepatocytes (Fig. 4F), demonstrating a significant impairment in the induced proliferative capacity of the *Rtel1*$^{K/K}$ hepatocytes with shortened telomeres.

DISCUSSION

RTEL1 was reported in 2004 as a regulator of telomere elongation, based on its genetic association with telomere length in crosses between the long-telomere species *M. musculus* and its short-telomere relative *M. spretus* [6]. However, the functional difference between the two RTEL1 proteins, which resulted in the different telomere length, has remained unknown [7]. Our previous discovery of an RTEL1 mutation in the conserved methionine 492 (M492I) as the cause for severe telomere shortening and the fatal human disease HHS, together with the finding that *M. spretus* RTEL1 has a lysine in this position suggested that this variation is responsible for the different telomere length of the two mouse species [8]. To examine this hypothesis, we derived a strain of *M. musculus* with a point mutation in *Rtel1*, replacing methionine 492 with a lysine, termed 'telomouse' (Fig. 1). Following the growth of MEFs derived from the *Rtel1*$^{K/K}$ mice over 250 population doublings revealed that their telomeres gradually shortened but otherwise they retained normal end-protection function and did not affect cell growth (Figs. 2 and S1-4). Distinct sharp bands of telomeric fragments, which are maintained clonally across more than 200 PD, indicated that the telomeres shortened because of insufficient telomerase action at telomeres, rather than by telomere deletion (Figs. 2A and S2,3). Slowing down the rate of shortening and the gradual disappearance of these bands suggested that when approaching the new telomere length set point, telomerase became more active and partially compensated for the shortening. Interestingly, the heterozygous *Rtel1*$^{M/K}$ MEFs displayed telomeres nearly as short as the homozygous *Rtel1*$^{K/K}$ MEFs (Fig. 2A,B), suggesting that the mutation is dominant in determining telomere length.

Interbreeding *Rtel1*$^{K/K}$ mice for seven generations revealed that in each generation telomeres shortened (Fig. 3C,D), suggesting a comparable shortening of the telomere length set point in the germline. The observed rate of shortening (2 to 0.3 kb per generation in tail, and 0.7 kb per generation in blood) is slower than the rate of shortening in the telomerase null (*mTR*$^{-/-}$) mouse (4.8 kb per generation) [21]. This suggests that telomerase is not entirely inactive in the *Rtel1*$^{K/K}$ mice, but it is regulated to reach a shorter steady-state length. Altogether, our results confirmed that the M492K

variation altered a function of RTEL1 in regulating telomere elongation, in line with other reports suggesting that RTEL1 regulates telomerase action at telomere ends [6,14,15,24].

What is the actual length of the telomeric repeat tracts in the 'telomouse' and in WT mice? In addition to the telomeric repeats tracts on the distal end of the chromosome, each terminal restriction fragment contains a subtelomeric region, extending from the most distal *HinfI* restriction site to the telomeric repeat tracts. Although *HinfI* is a frequent restriction endonuclease cutting a four base pair site, it is possible that this site is under-represented in subtelomeric regions if they are composed of low complexity sequences. To address this question, we examined the correlation between the telomeric hybridization signal and the measured length of the telomeric restriction fragments. Since equal amounts of genomic DNA samples were loaded on the gels, we expected the denatured hybridization signal within each gel to correlate with the telomere length – longer telomeres would bind more oligonucleotide probe. Plotting mean TRF length as a function of the telomeric hybridization signal indeed revealed a linear correlation (Fig. S6). Interestingly, however, extrapolation of the regression line indicated that the observed telomeric fragments are longer than expected from the signal by 10-15 kb, suggesting that mouse chromosomes have long subtelomeric sequences of low complexity with underrepresentation of *HinfI* restriction sites as compared to a random sequence. While this observation awaits a direct proof (e.g., by long-read sequencing), it suggests that mouse telomeres are actually not as long as the telomeric restriction fragments observed by in-gel hybridization. Thus, WT mice actually have 30-35 kb of telomeric repeat tracts (and not 50 kb) and the F10 tail samples actually contain only 8-13 kb of telomeric sequences. Furthermore, if nearly 40% of these telomeric fragments are below 20 kb, these fragments actually contain less than 5-10 kb of telomeric repeats (Fig. 3E). Altogether, according to this calculation, the telomeres of the late generation *Rtel1*$^{K/K}$ mice shortened to only a third of the WT telomere length (8-13 kb in F10 tail samples compared to 30-35 kb of the WT), and are well within the normal range of human telomere length.

Short telomeres are major drivers of the aging-dependent decline in organ function and increased cancer risk. Unfortunately, these processes have been difficult to study in the common laboratory mouse, *M. musculus,* due to its extremely long telomeres. So far attempts to study the implications of short telomeres in mice were based on telomerase null alleles, which cause ever-shortening telomeres and eventually result in severe pathologies and infertility, or on manipulating telomere proteins to induce overt telomere deprotection [2,25]. These existing mouse models are limited by the inability to maintain short but stable telomeres with normal, length-appropriate, function. The *Rtel1*^{M492K} 'telomouse' model is genetically identical to the common laboratory strain C57BL/6, except for a single amino acid difference in RTEL1. Yet, it displays dramatically shorter, near human-length telomeres with no signs of telomere dysfunction or phenotypes under normal physiological conditions, even in the fastest proliferating cells of the intestine or the male germline (Fig. 4A,B). When normally quiescent hepatocytes are forced to reenter the cell cycle and replicate multiple times, proliferative capacity was significantly reduced in the mutant hepatocytes (Fig. 4C-F). Future studies using the 'telomouse' model are promising to reveal the effects of short telomeres in various tissues on cell proliferation, age-related organ decay, and cancer development.

MATERIALS and METHODS

Derivation of Rtel1^{M492K} mice

All animal procedures were approved by and complied with the Animal Research Ethics Committees of the relevant institutions (the Hebrew University and the University of Pennsylvania). CRISPR guide RNAs were designed as described [26]. For sgRNA preparation, T7 sequence was added to the sgRNA template by PCR amplification using pX335 (Addgene #42335) with Phusion high-fidelity DNA Polymerase Kit (NEB) with Common primer and Primer 1 or Primer 2 (see below).

Common sgRNA-R: `5'-AGCACCGACTCGGTGCCACT-3'`

Primer 1 with gRNA sequence underlined:

TTAATACGACTCACTATAGG**CATCTGCATCTCCAGAGCAA**gttttagagctagaaatagc

Primer 2 with gRNA sequence underlined:

TTAATACGACTCACTATAGG**CACCTGGAGGTCACAACACT**gttttagagctagaaatagc

PCR products were purified using QIAquick Gel Extraction kit (Qiagen), followed by in vitro transcription using T7 High Yield RNA Synthesis kit (NEB). Newly synthesized sgRNAs were purified using the MEGAclear kit (Life Technologies), precipitated and diluted in injection buffer (10 mM Tris / 0.1 mM EDTA, pH 7.5) at the concentration of 500 ng/ul. The quality of the sgRNAs was bioanalyzed using the total RNA Nano Chip. Final injection mix was prepared using ssDNA repair template (IDT; 100 ng/ul; see below with mutated base underlined of the Methionine, bolded), sgRNA1 (50 ng/ul), sgRNA2 (50 ng/ul), Cas9 Nickase mRNA (Trilink; 100 ng/ul) in injection buffer. ssDNA repair template:

GTTCGTACCCTTATCCTCACCAGCGGTACCCTGGCTCCACTGTCTTCCTTTGCTCTGGAG**AAG**CAGATG

TATGTATGAGTCACCTGGAGGTCACAACACTAGGAACATGGTGGGTGGGGTTGG

The final mix was spun twice at top speed for 30 minutes at 4˚C to remove debris to avoid needle clogging. Cytoplasmic injection was done using C57Bl6 zygotes. After injection, SCR7 (Xcessbio) was added to the overnight egg culture at the concentration of 50 μM. Out of the 17 mice born, two had the targeted allele.

Preparation of MEF

Embryonic day (E)13.5 mouse embryos were dissected with head and inner organs removed, rinsed in HBSS, then digested with 300ul papain isolation enzyme (ThermoFisher) for 30 minutes at 37˚C following manufacture's protocol. In brief, embryonic juice was transferred to a conical tube with 1ml of HBSS, pipette up and down to achieve single cell suspension then spun. Pellet was re-suspended in MEF media (DMEM with 10% FCS, Pen/Strep/non essential amino acids) and plated.

Cell culture

MEFs were grown in DMEM media containing 2 mM L-glutamine, penicillin-streptomycin, non-essential AA and 20% fetal bovine serum until immortalization (around PD60-70) and then 10%. Media and media supplements were purchased from Biological Industries Inc., Beit Haemek, Israel.

Genomic DNA extraction

Leukocytes were obtained from blood by lysing red blood cells in 155 mM NH_4Cl, 10 mM $KHCO_3$ and 0.1 mM EDTA pH8 and precipitation. Leukocytes and MEFs were as lysed in 10 mM Tris pH 7.5, 10 mM EDTA, 0.15 M NaCl, 0.5% SDS and 100 µg/ml proteinase K overnight at 37˚C. Mouse tail samples were lysed in 100 mM Tris HCl pH8.5, 5 mM EDTA, 0.1% SDS, 200 mM NaCl and 100 µg/ml proteinase K overnight at 50˚C. Following cell lysis, high molecular weight genomic DNA was phenol extracted, ethanol precipitated, and dissolved in TE.

In-gel analysis of telomeric restriction fragments

Genomic DNA was treated with RNase A, digested with *HinfI* restriction endonuclease, and quantified by Qubit fluorometer. Equal amounts (3-5 µg) within each gel of the digested DNA samples were separated by pulsed-field gel electrophoresis (PFGE) using a Bio-Rad CHEF DR-II apparatus in 1% agarose and 0.5 x TBE, at 14˚C, 200V and pulse frequency gradient of 1 sec (initial) to 6 sec (final) for 22 hr (unless otherwise indicated). The gel was ethidium-stained, dried and hybridized as previously described [24], with a mixture of probes containing midrange PFG ladder (NEB Inc.) and 1 kb ladder (GeneDirex Inc.) that were digested with *HinfI* and dephosphorylated by quick calf intestine phosphatase (NEB Inc.), and a telomeric oligonucleotide, $(AACCCT)_3$. All probes were 5' end-labeled with [alpha-^{32}P]-ATP and T4 polynucleotide kinase (NEB Inc.). The gels were exposed to a PhosphorImager. TRF length was quantified using *TeloTool* (corrected mode) [27], individual band length was interpolated from regression formulas of the ladder bands size per migration distance, and

native and denatured in-gel hybridization intensity was quantified using *ImageQuant-TL* (GE Healthcare Inc.).

Immunofluorescence of cultured cells

Cells were seeded onto glass coverslips and grown for 1-4 days. Immunofluorescence was done as described [15]. Imaging was performed using FV-1200 confocal microscope (Olympus, Japan) with a 60X/1.42 oil immersion objective. *NIH ImageJ* [28] was used for image analysis and foci quantification.

Liver repopulation study

A total of 200,000 hepatocytes (100,000 from each *Rtel1*$^{K/K}$ mutant and UBC-GFP mouse; Jackson Laboratory #004353) were injected into the spleen of the FAH mice after removal of NTBC water. Procedures were followed as described [29]. At the end of the study, livers were harvested for evaluation using immunostaining and quantified using *NIH ImageJ* [28].

Statistical analysis

Statistical analysis was performed by Microsoft Excel and GraphPad Prism 8.0, using simple linear and polynomial nonlinear regression and two-tailed Student's t-test. p-values are indicated for the deviation of the slope from zero. $P < 0.05$ was considered statistically significant.

EdU Treatment

For EdU treatment, 150 µL of 10 mg/mL EdU solution was injected intraperitoneally two hours before mice were sacrificed.

Tissue Immunohistochemistry and Immunofluorescence

After euthanasia, mouse tissues were rinsed in PBS and fixed with 4% paraformaldehyde overnight. Fixed tissue was rinsed in PBS three times for 30 minutes per rinse and dehydrated for paraffin embedding and sectioning. EdU was detected according to the manufacturer's protocol (Click-iT EdU Calorimetric IHC Detection Kit C 10644, Molecular Probes). Briefly, tissue sections were deparaffinized and endogenous peroxidase enzymes were quenched using 3% hydrogen peroxide solution. Antigen retrieval was performed by incubating the tissue sections in Trypsin-EDTA solution for 30 minutes at room temperature. The tissue sections were then incubated in the Click-iT Edu Reaction Cocktail for 30 minutes at room temperature, washed, and treated with streptavidin-peroxidase conjugate for 30 minutes at room temperature. 3,3-diaminobenzidine tetra hydrochloride (DAB) was used as a substrate for the development of the signal. The following DAB incubation times were used for each tissue: 2.5 minutes for small intestine and colon, 4 minutes for gonads, and 8.5 minutes for liver and pancreas. Tissue sections were counter-stained with hematoxylin to visualize nuclei. For FAH and GFP staining, slides were subjected to heat antigen retrieval in a pressure cooker with Bulls Eye Decloaking buffer (Biocare). Slides were incubated in primary antibody overnight and secondary antibody conjugated to peroxidase, and then developed using Tyramide Signal Amplification (TSA, Akoya Biosciences). Primary antibodies used for staining were: Rabbit anti-FAH (ThermoFisher; PA542049) and Goat anti-GFP (Abcam; AB6673). TSA-conjugated secondary antibodies (Cy2 and Cy3) were used. Images were taken using a Keyence All-in-One Fluorescence BZ-X800 microscope with brightfield capabilities. Animals were assigned to condition by genotype and were age-matched mice from the same colony.

REFERENCES

1. Maciejowski, J. & de Lange, T. Telomeres in cancer: tumour suppression and genome instability. *Nat Rev Mol Cell Biol* **18**, 175-186 (2017).
2. Chakravarti, D., LaBella, K.A. & DePinho, R.A. Telomeres: history, health, and hallmarks of aging. *Cell* **184**, 306-322 (2021).
3. Roake, C.M. & Artandi, S.E. Regulation of human telomerase in homeostasis and disease. *Nat Rev Mol Cell Biol* **21**, 384-397 (2020).
4. Zhu, L. *et al.* Telomere length regulation in mice is linked to a novel chromosome locus. *Proc Natl Acad Sci U S A* **95**, 8648-53 (1998).
5. Kim, S.H., Parrinello, S., Kim, J. & Campisi, J. Mus musculus and Mus spretus homologues of the human telomere-associated protein TIN2. *Genomics* **81**, 422-32 (2003).
6. Ding, H. *et al.* Regulation of murine telomere length by Rtel: an essential gene encoding a helicase-like protein. *Cell* **117**, 873-86 (2004).
7. Lansdorp, P. & van Wietmarschen, N. Helicases FANCJ, RTEL1 and BLM Act on Guanine Quadruplex DNA in Vivo. *Genes (Basel)* **10**(2019).
8. Deng, Z. *et al.* Inherited mutations in the helicase RTEL1 cause telomere dysfunction and Hoyeraal-Hreidarsson syndrome. *Proc Natl Acad Sci U S A* **110**, E3408-16 (2013).
9. Glousker, G., Touzot, F., Revy, P., Tzfati, Y. & Savage, S.A. Unraveling the pathogenesis of Hoyeraal-Hreidarsson syndrome, a complex telomere biology disorder. *Br J Haematol* **170**, 457-71 (2015).
10. Savage, S.A. Beginning at the ends: telomeres and human disease. *F1000Res* **7**(2018).
11. Vannier, J.B., Pavicic-Kaltenbrunner, V., Petalcorin, M.I., Ding, H. & Boulton, S.J. RTEL1 Dismantles T Loops and Counteracts Telomeric G4-DNA to Maintain Telomere Integrity. *Cell* **149**, 795-806 (2012).
12. Vannier, J.B. *et al.* RTEL1 is a replisome-associated helicase that promotes telomere and genome-wide replication. *Science* **342**, 239-42 (2013).
13. Margalef, P. *et al.* Stabilization of Reversed Replication Forks by Telomerase Drives Telomere Catastrophe. *Cell* **172**, 439-453 e14 (2018).
14. Uringa, E.J. *et al.* RTEL1 contributes to DNA replication and repair and telomere maintenance. *Mol Biol Cell* **23**, 2782-2792 (2012).
15. Awad, A. *et al.* Full length RTEL1 is required for the elongation of the single-stranded telomeric overhang by telomerase. *Nucleic Acids Res* **48**, 7239-7251 (2020).
16. Prowse, K.R. & Greider, C.W. Developmental and tissue-specific regulation of mouse telomerase and telomere length. *Proc Natl Acad Sci U S A* **92**, 4818-22 (1995).
17. Vaziri, H. & Benchimol, S. Reconstitution of telomerase activity in normal human cells leads to elongation of telomeres and extended replicative life span. *Curr Biol* **8**, 279-82 (1998).
18. de Lange, T. Shelterin-Mediated Telomere Protection. *Annu Rev Genet* **52**, 223-247 (2018).

19. Di Micco, R. *et al.* DNA damage response activation in mouse embryonic fibroblasts undergoing replicative senescence and following spontaneous immortalization. *Cell Cycle* **7**, 3601-6 (2008).

20. Lamm, N. *et al.* Diminished telomeric 3' overhangs are associated with telomere dysfunction in Hoyeraal-Hreidarsson syndrome. *PLoS One* **4**, e5666 (2009).

21. Blasco, M.A. *et al.* Telomere shortening and tumor formation by mouse cells lacking telomerase RNA. *Cell* **91**, 25-34. (1997).

22. Lee, H.W. *et al.* Essential role of mouse telomerase in highly proliferative organs. *Nature* **392**, 569-74 (1998).

23. Grompe, M. Fah Knockout Animals as Models for Therapeutic Liver Repopulation. *Adv Exp Med Biol* **959**, 215-230 (2017).

24. Porreca, R.M. *et al.* Human RTEL1 stabilizes long G-overhangs allowing telomerase-dependent over-extension. *Nucleic Acids Res* **46**, 4533-4545 (2018).

25. Li, H. *et al.* Mouse models in modeling aging and cancer. *Exp Gerontol* **120**, 88-94 (2019).

26. Yang, H., Wang, H. & Jaenisch, R. Generating genetically modified mice using CRISPR/Cas-mediated genome engineering. *Nat Protoc* **9**, 1956-68 (2014).

27. Gohring, J., Fulcher, N., Jacak, J. & Riha, K. TeloTool: a new tool for telomere length measurement from terminal restriction fragment analysis with improved probe intensity correction. *Nucleic Acids Res* **42**, e21 (2014).

28. Rasband, W.S. ImageJ. (U. S. National Institutes of Health, Bethesda, Maryland, USA, http://imagej.nih.gov/ij/, 1997-2014).

29. Reizel, Y. *et al.* FoxA-dependent demethylation of DNA initiates epigenetic memory of cellular identity. *Dev Cell* **56**, 602-612 e4 (2021).

ACKNOWLEDGMENTS

We are grateful to all members of the Tzfati and Kaestner laboratories for stimulating discussions and assistance. We thank Ittai Ben-Porath and Amir Eden for the gifts of WT mice and MEFs, Devora Olam for assistance in mouse blood collection, Naomi Melamed-Book for assistance with confocal imaging, Dana Avrahami-Tzfati for assistance with CRISPR, and Ran Avrahami for assistance with statistical analyses. We thank the University of Pennsylvania's Diabetes Research Center (DRC) for the use of the Functional Genomics Core (P30-DK019525) and the Center for Molecular Studies in Digestive and Liver Diseases for the use of the Molecular Pathology and Imaging and Transgenic and

Chimeric Mouse Cores (P30-DK050306). We also thank Lan Cheng in IDOM Histology Service for performing the IF staining, and Ayano Kondo for writing a code for *ImageJ* analysis.

FUNDING

Israel Science Foundation grant 2071/18 (YT)

National Institute of Diabetes and digestive and Kidney grant R37-DK053839 (KHK)

British Council Israel-UK-Palestine GROWTH Fellowship (RS)

AUTHOR CONTRIBUTIONS

Conceptualization: YT, KHK, RS

Methodology: RS, CLM, YR

Investigation: RS, CLM, HK, YR, AM

Funding acquisition: YT, KHK, RS

Supervision: YT, KHK

Writing and revising – YT, KHK, RS, CLM, YR

COMPETING INTERESTS

Authors declare that they have no competing interests.

SUPPLEMENTARY MATERIALS

Supplementary Figs. S1 to S6

Tables S1 and S2

FIGURES

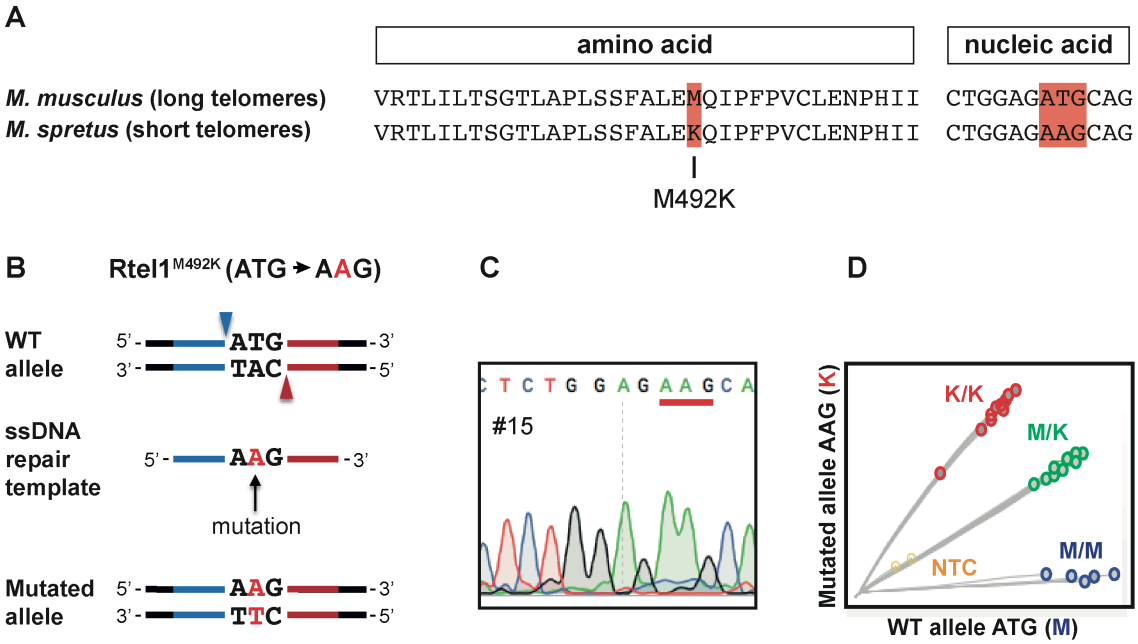

Fig. 1. Generation of Rtel1^{M492K} allele using CRISPR-Cas9 Nickase editing strategy. (**A**) Evolutionary conservation of part of the RTEL1 protein between *M. musculus* and *M. spretus* with the mutated methionine 492 and the corresponding nucleic acid codon highlighted in red. (**A**) Illustration showing WT allele, two gRNAs targeted positions (blue and red arrowheads), ssDNA repair template with the mutation, left homology arm (blue), right homology arm (red) and the resulting targeted allele. (**C**) Sanger sequencing of founder #15 confirming the replacement of the "T" with an "A" at the codon encoding methionine 492, changing it to a lysine (underlined). (**D**) Genotyping of animals using Custom Taqman SNP Genotyping Assays. M/M (wild-type; blue), M/K (heterozygotes; green), K/K (homozygotes; red), and NTC (no-template-control; yellow).

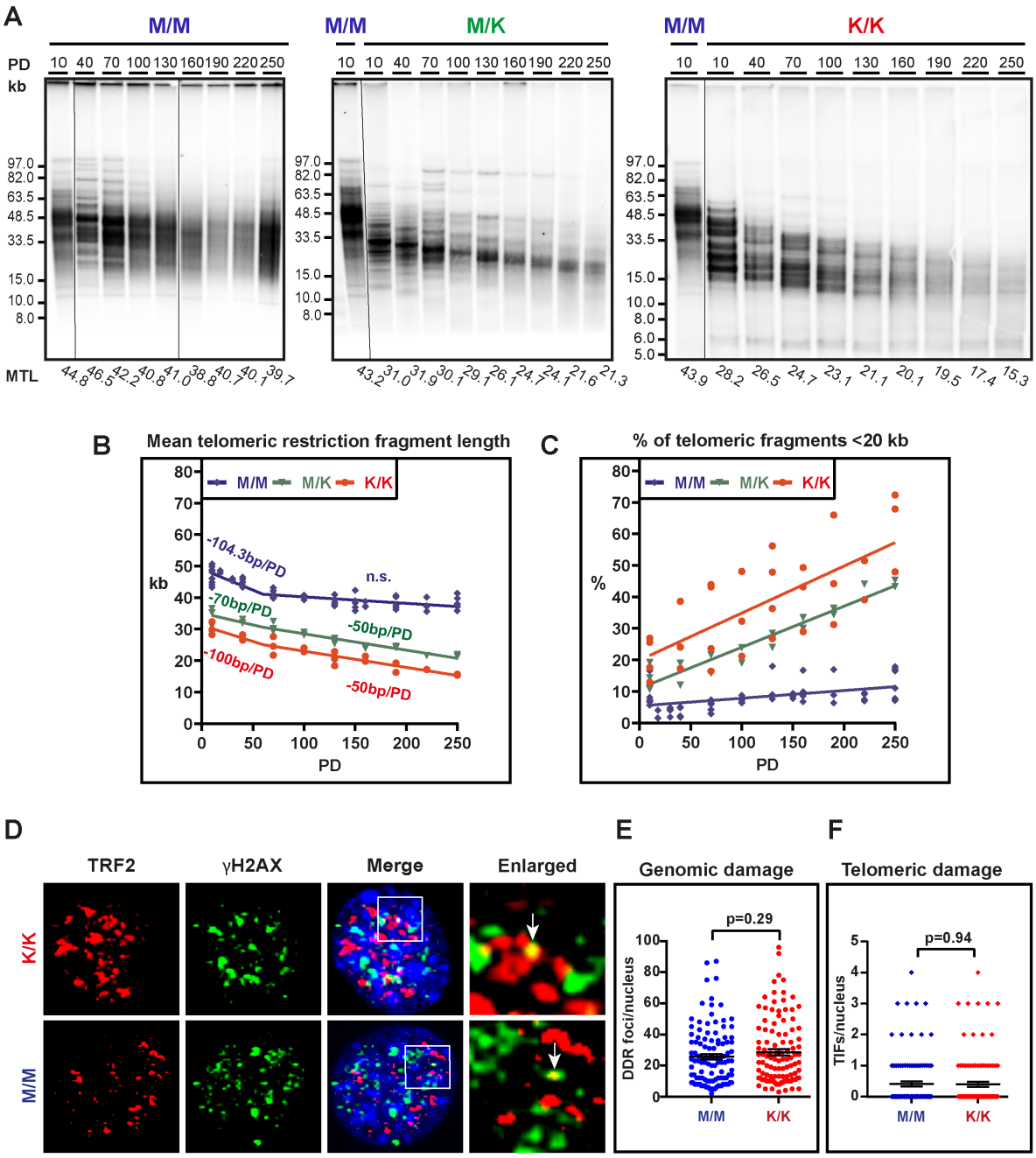

Figure 2. Telomeres of the MEFs carrying the *Rtel1*^{M492K} mutation progressively shorten in culture. (**A**) Genomic DNA samples prepared from WT (M/M) or *Rtel1*^{M492K} mutant, homozygous (K/K) or heterozygous (M/K), MEF cultures, were analyzed by PFGE and in-gel hybridization to the denatured DNA as described under Supplementary Materials and Methods, except for the gel on the right, which was electrophoresed for less time (18 h). Mean telomere length was quantified by *TeloTool* [27] and indicated below the lanes. (**B**) Each sample was repeatedly measured in additional gels (summarized in Supplementary Table 1) and plotted. (**C**) The percentage of telomeric fragments shorter than 20 kb for each sample was calculated from the mean and standard deviation of TRF lengths obtained by *TeloTool* (Supplementary Table 1) and plotted. (**D**) The formation of DDR foci and their localization to telomeres (defined as TIF) were tested by immunofluorescence with antibodies detecting the DDR marker γH2AX (green) and the telomere protein TRF2 (red). White arrows indicate TIF. (**E,F**) Scatter plots showing the number of DDR foci and TIF per nucleus. The mean and standard error of the mean (SEM) for each culture are indicated by black lines. n=110 nuclei for each culture.

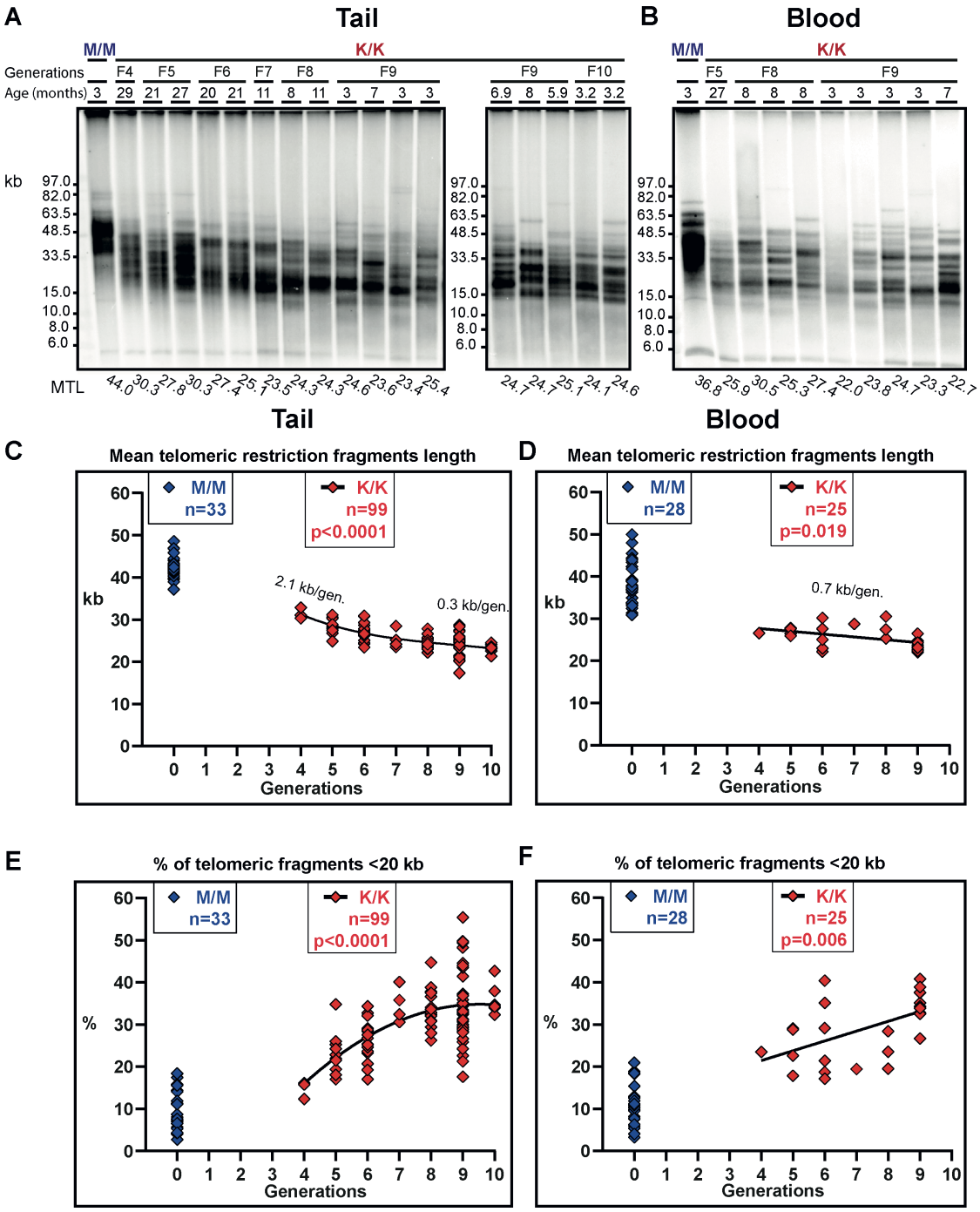

Figure 3. Telomeres of mice carrying the *Rtel1*^{M492K} mutation progressively shorten over generations. Genomic DNA samples prepared from mutant (K/K) or WT (M/M) mice tail samples (**A**) or blood leukocytes (**B**) at the indicated generations and ages were analyzed by PFGE and in-gel hybridization to the denatured DNA. (**C,D**) Tail and blood mean TRF length for each generation was repeatedly measured in additional gels and plotted. Rates of telomere shortening per generation were calculated from the best-fit regression lines (2nd order polynomial for tail and linear for blood). P values indicated the deviation of the linear regression slope from 0. (**E,F**) The percentage of telomeric fragments shorter than 20 kb for each sample was calculated from the mean and standard deviation of TRF lengths obtained by *TeloTool* [27]. n, number of samples analyzed. All data are summarized in Supplementary Table 2.

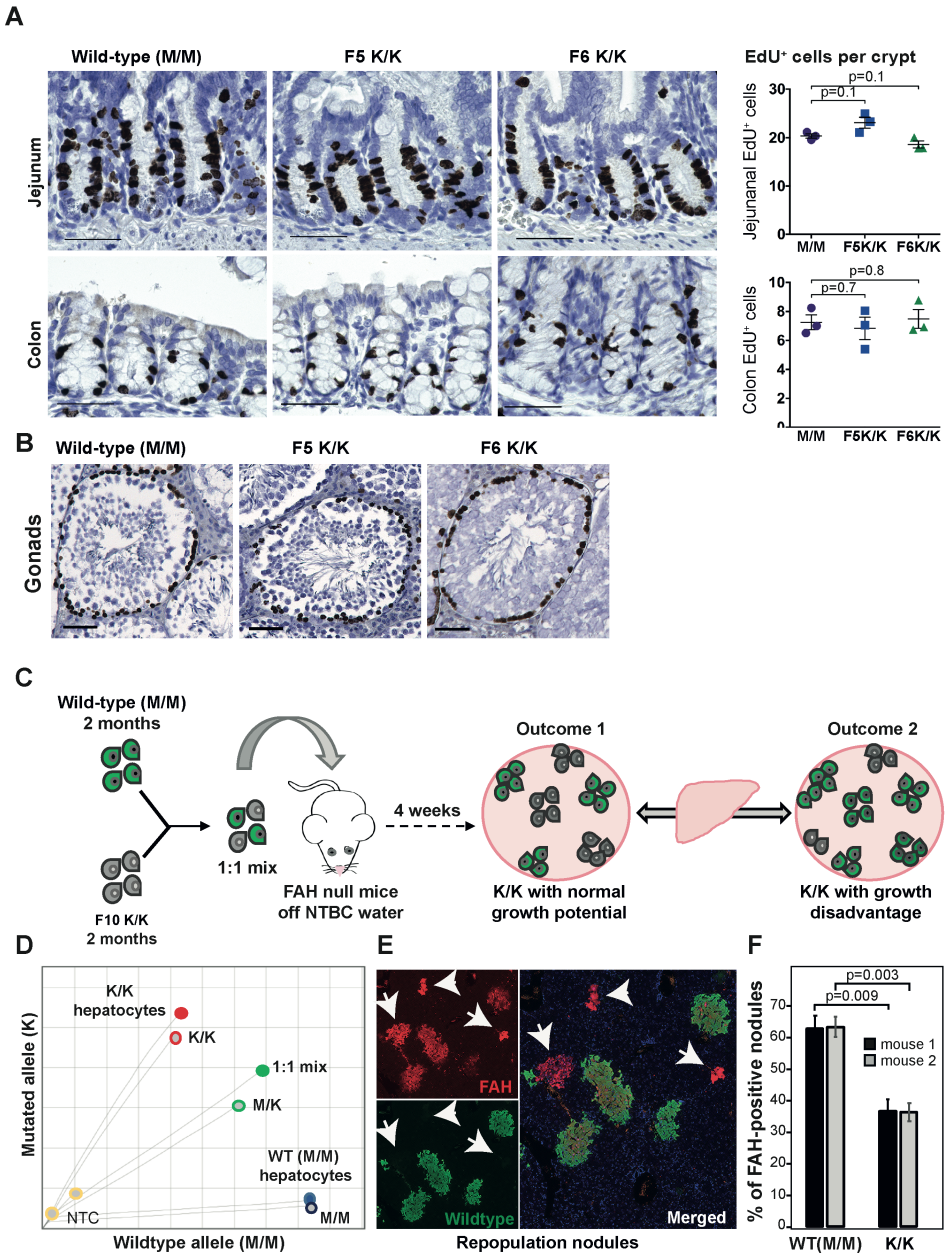

Figure 4. **The *Rtel1*^{M492K} mice display decreased liver repopulation capacity.** (**A**) Intestinal crypt stem and progenitor cells in the jejunum and colon of *Rtel1*$^{K/K}$ mice (F5 and F6) display proliferation rates indistinguishable from the WT (M/M), as revealed by short-term (90 minutes) EdU labeling. (**B**) Testes of K/K mice display the normal arrangement of proliferating spermatogonia in the seminiferous tubules. (**C**) Scheme for the competitive hepatocyte repopulation study. WT (M/M) GFP-positive hepatocytes and mutant (F10 K/K) GFP-negative hepatocytes were mixed in a 1:1 ratio and transplanted into FAH null mice. After removal of the protective drug, NTBC, host hepatocytes died and transplanted hepatocytes were forced to re-enter the cell cycle and proliferate rapidly. (**D**) TaqMan assay of the mixed hepatocytes confirms equal numbers of each genotype. (**E**) A representative liver section immunostained red for FAH protein (all nascent repopulation nodules) and in green for GFP (only the WT repopulation hepatocytes). White arrows indicate GFP-negative repopulation nodules from the K/K mutant donor mouse. Note that the WT (green) hepatocytes are overrepresented. (**F**) GFP-negative hepatocytes from K/K mutant F10 mice displayed a 45% reduction in the number of repopulation nodules compared to GFP-positive WT. Graphs indicate SEM.